Journal of Solid State Chemistry **159,** 362–370 (2001)
doi:10.1006/jssc.2001.9166, available online at http://www.idealibrary.com on IDEAL®

Layered Mixed-Metal Phenylphosphonates, $Mn_xCo_{1-x}(O_3PC_6H_5)\cdot H_2O$: Structure and Magnetic Properties

Jeffrey T. Culp,* Gail E. Fanucci,*,[1] Brian C. Watson,† A. Nicole Morgan,† Rénal Backov,* Hitoshi Ohnuki,*,[2] Mark W. Meisel,†,[3] and Daniel R. Talham*,[3]

*Department of Chemistry; and †Department of Physics and Center for Ultralow Temperature Research, University of Florida, Gainesville, Florida 32611-7200
E-mail: talham@chem.ufl.edu

Received March 20, 2001; accepted March 21, 2001

IN DEDICATION TO THE LATE PROFESSOR OLIVIER KAHN FOR HIS PIONEERING CONTRIBUTIONS TO THE FIELD OF MOLECULAR MAGNETISM

Mixed metal phenylphosphonates of composition $Mn_xCo_{1-x}(O_3PC_6H_5)\cdot H_2O$ were prepared with $0 \le x \le 1$. Atomic absorption, X-ray powder diffraction, and electron paramagnetic resonance measurements indicate that the mixed-metal solid solutions are homogeneous and isostructural with the single-metal-parent compounds over the entire concentration range, with a small, systematic evolution of the *a* and *c* in-plane unit cell parameters. The temperature dependence of the magnetic data for the pure Mn^{2+} ($x = 1$) and pure Co^{2+} ($x = 0$) samples was fitted by standard 2D Heisenberg and 2D Ising models, respectively, yielding nearest-neighbor exchange interaction energies of $J = -2.27 \pm 0.02$ K for $Mn(O_3PC_6H_5)\cdot H_2O$ and $J = -2.43 \pm 0.05$ K for $Co(O_3PC_6H_5)\cdot H_2O$. The magnetic phase diagram, down to 2 K, was constructed over the entire composition range. Both dc and ac magnetic susceptibilities were used to identify the transitions to low temperature, long-range-ordered antiferromagnetic states. In the Mn^{2+}- and Co^{2+}-rich regions, the ordering temperature, T_N, decreases relative to the pure materials, as expected for magnetic ion impurity doping. For intermediate values of *x*, Mn^{2+}–Mn^{2+} interactions dominate, resulting in a minimum in T_N near $x = 0.25$. A weak negative magnetization was observed for $x < 0.25$. No evidence of spin glass behavior was observed for any concentration at any temperature.

Key Words: **magnetic phase diagram; canted antiferromagnet; mixed-metal; solid solution; manganese; cobalt; phenylphosphonate; magnetism.**

INTRODUCTION

Even before Clearfield's and Smith's elucidation of the structure of the prototype α-$Zr(HPO_4)_2\cdot H_2O$ (1), layered metal phosphates were extensively studied primarily because of their ion exchange capabilities (2). This initial interest has been extended to metal phosphonates where similar architectures are found (3–7) and now includes organic networks that can be varied to further modify the properties of the layered solids (8–13). Recently, layered metal phosphates and phosphonates have been shown to exhibit interesting magnetic phenomena, including magnetic ordering, canted antiferromagnetism (14–21), and antiferromagnetic resonance (22), and they have been studied as models for two-dimensional (2D) magnetism. Our group has also extended these studies from the solid-state (22, 23), to monolayer (24–27) and multilayer thin films (28–33), where similar properties have been observed.

As part of our interest in 2D magnetism in metal phosphonate solids and thin films, we have investigated a series of mixed-metal Mn^{2+}/Co^{2+} and Mn^{2+}/Zn^{2+} phenylphosphonates. Two possibilities exist if mixed metal phases form, each giving rise to different magnetic behavior. If ions of a different spin state organize in an ordered fashion, then a new superstructure is formed, giving rise to the possibility of ferrimagnetism if the spin state of the two ions is different. Alternatively, if the ions distribute randomly, then a solid solution results. Historically, mixed-metal solid solutions have been extensively studied (34) because they exhibit altered magnetic behavior and provide an opportunity for studying the details of magnetic ordering mechanisms. Systems based on Mn^{2+}/Co^{2+} have been popular choices, as the materials cover a range of dimensions, from quasi-1D (35–37) to quasi-2D (38) to 3D (39), and in most cases an isotropic (Heisenberg-type) interaction describes the coupling between $S = \frac{5}{2}$ spins of Mn(II) ions, while an anisotropic (Ising-type) interaction describes the coupling between "effective" $S = \frac{1}{2}$ spins of Co(II). Consequently, upon dilution these materials experience an interesting blend of competing spin and lattice dimensions. Despite previous studies on mixed-metal solids, there are still some unanswered

[1] Current address: Department of Chemistry, University of Virginia, Charlottesville, VA 22904–4319.

[2] Current address: Tokyo University Mercantile Marine, Applied Physics Laboratory, Koto Ku, Etchujima 2-1-6, Tokyo 1358533, Japan.

[3] To whom correspondence should be addressed.

0022-4596/01 $35.00

questions. For example, in some cases, but not all, the combination of random mixing and magnetic frustration leads to spin glass behavior (40). In addition, some ferrimagnetic systems have exhibited the interesting effect of negative magnetization (41, 42). New examples of mixed-metal magnetic systems, either structurally ordered or as solid solutions, can provide the opportunity to further study some of these phenomena.

The divalent metal phenylphosphonates form an isostructural series (Fig. 1) (5), and we find that the mixed-metal analogues form as solid solutions of formula $Mn_xCo_{1-x}(O_3PC_6H_5)\cdot H_2O$ or $Mn_xZn_{1-x}(O_3PC_6H_5)\cdot H_2O$. At low temperature, the pure Mn^{2+} and pure Co^{2+} phenylphosphonates experience long-range antiferromagnetic order at $T_N \approx 12$ and 4 K, respectively. Upon dilution, the ordering temperatures are reduced compared to the values found for the pure compounds, and the resulting magnetic phase diagrams are reported here. For diamagnetic Zn^{2+} doping, i.e., Mn_xZn_{1-x}, the reduction of T_N follows the prediction of mean field theory for $x > 0.6$ and this magnetic phase diagram was reported previously (43). However, for the Mn_xCo_{1-x} compounds, the reduction of T_N with doping concentration is weaker than expected on the basis of mean field theory. For Mn_xCo_{1-x} at low temperatures, the magnetization of the Mn-rich specimens, i.e., $x > 0.25$, is characterized by canted antiferromagnetic behavior. On the other hand, the magnetization of the Co-rich specimens, i.e., $x < 0.25$, exhibits a very small negative magnetization behavior when the zero-field cooled and field-cooled data are compared. The magnetic phase diagram for $Mn_xCo_{1-x}(O_3PC_6H_5)\cdot H_2O$ is reported here.

EXPERIMENTAL

Materials used. Reagent grade $Mn(NO_3)_2\cdot 4H_2O$, $CoCl_2\cdot 6H_2O$ and phenylphosphonic acid ($C_6H_5PO_3H_2$, 95%) were purchased from Aldrich (Milwaukee, WI) and used without further purification. The water used in all reactions was purified with a Barnstead NANOpure purification system that produced water with an average resistivity of 18 MΩ cm. $Mn(O_3PC_6H_5)\cdot H_2O$ and $Co(O_3PC_6H_5)\cdot H_2O$ were synthesized by mixing equimolar amounts of the appropriate metal ion solution with a solution of phenylphosphonic acid (pH adjusted to 5–6 with 0.1 M KOH) both heated to 60°C prior to mixing. The solutions were allowed to stir for 2 h at this temperature. For each sample, the precipitate was filtered, washed with water and subsequently with acetone, and then dried under vacuum.

Preparation of $Mn_xCo_{1-x}(O_3PC_6H_5)\cdot H_2O$ compounds. The mixed-metal phenylphosphonates $Mn_xCo_{1-x}(O_3PC_6H_5)\cdot H_2O$ were prepared in a manner similar to that of the pure metal phenylphosphonates but with slight modification. In each case, aqueous solutions of the metal salts in the desired molar ratios were heated to 60°C and added to a solution containing a slight excess of phenylphosphonic acid at pH 5–6. The resultant solutions were stirred for only 10 min. before filtering the precipitate. The products were washed with water and acetone, and finally dried under vacuum. In all cases, the final Mn:Co ratios (determined by atomic absorption) of the solid-state materials were similar, i.e., within 10%, to those of the starting metal salt solutions.

Instrumentation. Atomic absorption (AA) measurements were performed on a Perkin–Elmer Model 3100 atomic absorption spectrometer with a photomultiplier tube detector. For AA analysis, the solid-state samples were dissolved in a 1.0 M HCl solution. X-ray diffraction was done with a step scan (0.02° 2θ/step, 2 s/step) using a Phillips APD 3720 X-ray powder diffractometer with the Cu$K\alpha$ line as the source. Electron paramagnetic resonance (EPR) spectra were recorded on a Bruker (Billerica, MA) ER 200D spectrometer modified with a digital signal channel and a digital field controller. Data were collected using a U.S. EPR (Clarksville, MD) SPEC300 data acquisition program and converted to ASCII format using a U.S. EPR EPRDAP data analysis program. Magnetization and ac susceptibility measurements were performed using a Quantum Design MPMS SQUID magnetometer. The dc measurements were made with a measuring field of 100 G or 1.0 kG when sweeping the temperature, or were made at 2 K while sweeping the field up to 50 kG. The ac susceptibility measurements used frequencies ranging from 17 Hz to 1.5 kHz and an ac field amplitude of 4.0 G. Additional low-frequency (19 Hz) ac susceptibility measurements were performed with a homemade mutual inductance coil of a standard design (44). High-frequency (14 MHz) studies were conducted in a homemade tank-circuit biased with tunnel diode (44, 45). For all of the magnetic studies, powder samples were contained in gelcaps or plastic vials, with the exception of the work performed at 14 MHz when the sample was loaded directly into the housing of the coil. The background signals arising from the gelcaps and vials were independently measured and were either negligible or subtracted from the data.

RESULTS AND DISCUSSION

Sample preparations. In order to encourage homogeneous solid solutions of composition $Mn_xCo_{1-x}(O_3PC_6H_5)\cdot H_2O$, and to prevent any annealing into a multiphased system, samples were quickly precipitated and collected immediately. This procedure resulted in a decreased crystallinity of the solid solutions, relative to what is possible with the pure phases, although it is sufficient for powder XRD analyses and does not appear to influence the magnetic properties. All attempts to prepare mixed-metal

samples of high crystallinity by slow-growth techniques resulted in the formation of physical mixtures and/or multiphase materials.

Structural characterizations. The relative percentage of manganese and cobalt in the solid solutions was determined from AA analyses (Table 1). Although AA spectroscopy gives an average stochiometry, it cannot provide information about the structural homogeneity of the samples. Therefore, X-ray diffraction was used to determine if the final product consists of single or multiple phases. The structures of the pure manganese and cobalt phenylphosphonate compounds consist of layers of quasi-two-dimensional metal-phosphorus-oxygen sheets that define the *ac* plane, while the organic moieties project between the layers, thus defining the *b* axis (Fig. 1) (4, 5). These materials are known to crystallize in the same space group, $Pmn2_1$, with slight modifications of the *ac* basal plane spacings (4, 5). However, the interplane distances are almost identical because both compounds contain the same organic phenyl group.

Due to the symmetry of the $Pmn2_1$ space group, the 100 and 001 reflections are systematically absent, so the highest order reflections containing in-plane structural information are the 110 and 011. Although both of these reflections contain an interplane contribution, this distance remains essentially constant for all compositions. The 110, 030, and 011 reflections conveniently occur consecutively over a small range of 2θ in the X-ray diffractogram, making them a practical series for monitoring variations in the *ac* lattice spacings. The position of the 030 reflection in all samples is an internal reference that confirms that the interplane distances do not change as a function of doping, allowing the 2θ values for the 110 and 011 reflections in the doped materials to be used to determine the in-plane lattice spacings.

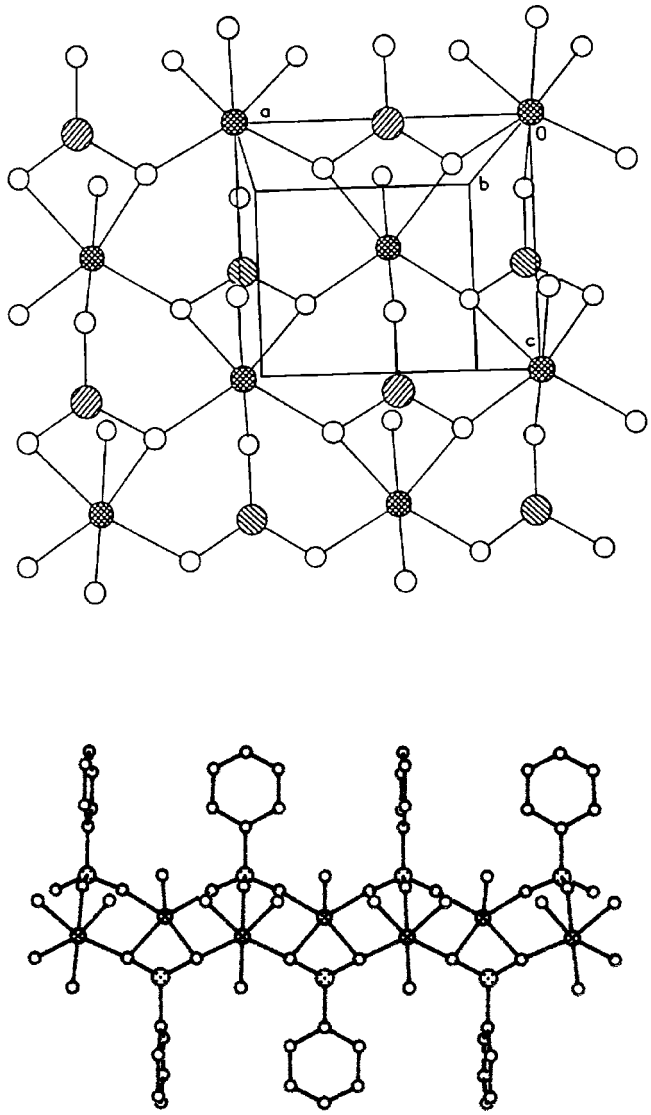

FIG. 1. In-plane and cross-sectional view of $Mn(O_3PC_6H_5)\cdot H_2O$. Crystallographic data are taken from Ref. (5). Key: oxygen, small open circles; manganese, cross-hatched circles; phosphorus, diagonal-hatched circles (phosphorus atoms above and below the plane are distinguished by hatches with different directions).

TABLE 1

Concentration of Manganese in $Mn_xCo_{1-x}(O_3PC_6H_5)\cdot H_2O$ Determined from AA Spectroscopy and Unit Cell Parameters from the 110, 011, and 030 *hkl* Reflections in the Corresponding Powder XRD Patterns

Mol % Mn	$a \pm 0.01$	$b \pm 0.01$	$c \pm 0.01$
100	5.73	14.34	4.94
95	5.73	14.34	4.94
82	5.70	14.34	4.92
68	5.68	14.34	4.90
55	5.66	14.34	4.88
35	5.65	14.34	4.88
30	5.64	14.34	4.87
21	5.62	14.34	4.86
19	5.63	14.34	4.85
11	5.61	14.34	4.85
10	5.61	14.34	4.85
0	5.60	14.34	4.83

Powder XRD patterns for the pure manganese and pure cobalt phenylphosphonates, as well as that of the $Mn_{0.35}Co_{0.65}$ sample, are shown in Fig. 2. The similarity of the patterns in Fig. 2A makes it clear that the mixed-metal systems are isostructural with the parent compounds. An expansion of the region between 2θ values of 16°–20° in Fig. 2B shows the 110, 030, and 011 reflections for the same three compounds. For the mixed-metal example, discrete 110 and 011 reflections are observed at 2θ values between those of the pure Mn^{2+} and Co^{2+} phases, while the 030

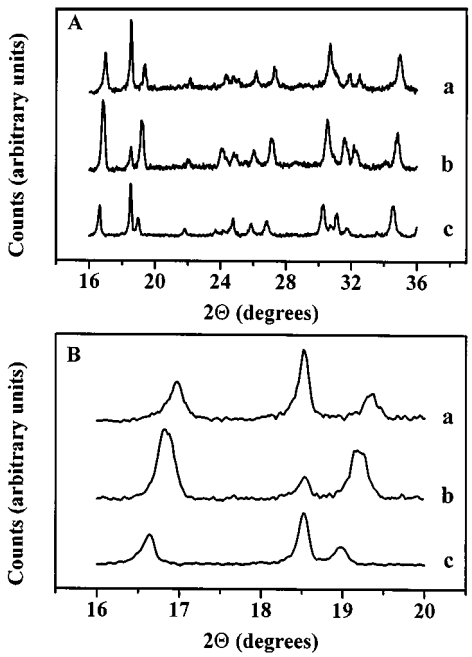

FIG. 2. (A) XRD powder patterns for (a) $Co(O_3PC_6H_5)\cdot H_2O$, (b) $Mn_{0.35}Co_{0.65}(O_3PC_6H_5)\cdot H_2O$, and (c) $Mn(O_3PC_6H_5)\cdot H_2O$. (B) Expansion showing, from left, 110, 030, 011 *hkl* reflections for (a) $Co(O_3PC_6H_5)\cdot H_2O$, (b) $Mn_{0.35}Co_{0.65}(O_3PC_6H_5)\cdot H_2O$, and (c) $Mn(O_3PC_6H_5)\cdot H_2O$.

reflection remains the same for all three samples. These observations are consistent with the formation of a single homogeneous solid solution. Similar results were seen for all compositions, and Table 1 lists the corresponding *a*, *b*, *c* cell parameters for the pure and doped materials as calculated from the 110, 030, and 011 reflections. The cell edge lengths systematically shift in value as a function of *x*. The absence of any reflections corresponding to the pure single-ion phenylphosphonates in the XRD patterns of the mixed-metal phenylphosphonates, combined with the observation that the detected reflections have 2θ values between those of the two pure compounds, provides convincing evidence that single-phase solid solutions have been formed.

Electron paramagnetic resonance. Evidence for microscopic homogeneity of the solid solutions comes from EPR. The cobalt phosphonate is EPR silent at X-band, while the manganese analog gives a broad line that is structureless as a result of dipolar interactions (Fig. 3) (46). The anisotropy of the EPR linewidth has previously been used to demonstrate the two-dimensional exchange pathways in the layered manganese phosphonates (23, 46). As the percentage of Co^{2+} in the solid solution increases, the Mn^{2+} signal broadens (Fig. 3), reflecting the randomization of the identity of the Mn^{2+} ion's nearest neighbors. In the solid solution, there is no signal due to crystallites of pure $Mn(O_3PC_6H_5)\cdot H_2O$.

Magnetic properties of $Mn(O_3PC_6H_5)\cdot H_2O$ *and* $Co(O_3PC_6H_5)\cdot H_2O$. The magnetic properties of several manganese and cobalt organophosphonates have been studied previously (15, 16, 18, 19, 22). The manganese phosphonates undergo a long-range ordering transition to a canted antiferromagnetic state at temperatures ranging from 12 to 18 K, depending on the identity of the organophosphonate. Pure $Mn(O_3PC_6H_5)\cdot H_2O$ orders at $T_N \approx 12$ K (22). The cobalt phosphonates also order antiferromagnetically, and for $Co(O_3PC_6H_5)\cdot H_2O$, we observe $T_N \approx 4$ K, as we describe later in this section.

The data in Fig. 4 show the temperature dependence of the static magnetic susceptibility of the pure Mn and Co materials, acquired by cooling the samples in zero magnetic field and measuring in a dc field of 1 kG. The broad maximum in the susceptibility, χ_{max}, is characteristic of low-dimensional antiferromagnetic interactions when short-range order correlations become greater than the thermal fluctuations of the spins. These short-range correlations are established by magnetic exchange interactions, *J*, which are typically considered to be limited to nearest neighbor spins. In other words, the Hamiltonian may be written as

$$\mathscr{H} = -J\sum_{nn} \mathbf{S}_i\cdot\mathbf{S}_j, \qquad [1]$$

where $\sum_{nn}$ runs over all pairs of nearest neighbor spins $\mathbf{S}_i$ and $\mathbf{S}_j$. The susceptibility data for the manganese phosphonate may be fitted with a 2D high-temperature series expansion (47) for a quadratic layer of Heisenberg $S = \frac{5}{2}$ spins based on Eq. [1], and the solid line in Fig. 4A shows the best fit to the data with $J = -2.27 \pm 0.02$ K. The fit was restricted to $T > 20$ K since at lower temperatures the

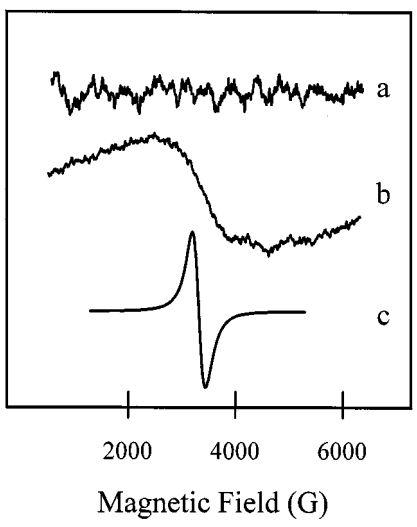

FIG. 3. Room temperature EPR signals for (a) $Co(O_3PC_6H_5)\cdot H_2O$, (b) $Mn_{0.84}Co_{0.16}(O_3PC_6H_5)\cdot H_2O$, and (c): $Mn(O_3PC_6H_5)\cdot H_2O$.

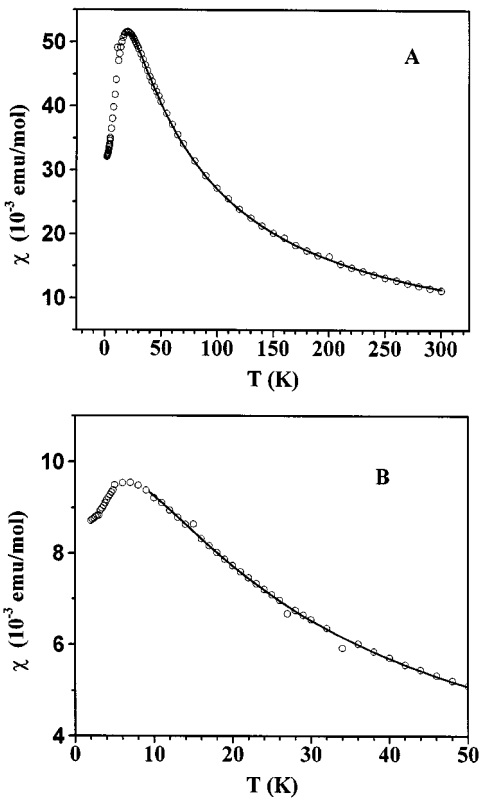

FIG. 4. (A) The temperature dependence of the DC magnetic susceptibility for $Mn(O_3PC_6H_5)\cdot H_2O$ after zero field cooling the specimen to 2 K and then measuring in a field of 1 kG. The results of a fit using a $S = \frac{5}{2}$ Heisenberg high-temperature expansion for $T > 20$ K are shown by the solid line with the result $J = -2.27 \pm 0.02$ K, as described in the text. (B) The temperature dependence of the DC magnetic susceptibility for $Co(O_3PC_6H_5)\cdot H_2O$ after zero-field cooling the sample to 2 K and then measuring in a field of 1 kG. The results of a fit using an $S = \frac{1}{2}$ Ising high-temperature expansion for $T > 9.5$ K are shown by the solid line with the result $J = -2.43 \pm 0.05$ K, as described in the text.

fitting procedure is not valid. In the case of the pure cobalt phenylphosphonate, Eq. [1] still describes the simplest interactions for the case of this 2D, $S = \frac{1}{2}$ Ising system when the spin operators are restricted to their z components (48). The solid line in Fig. 4B is a fit, for $T > 9.5$ K, to a 2D, $S = \frac{1}{2}$ Ising high-temperature series expansion (49), using an exchange constant of $J = -2.43 \pm 0.05$ K. It is noteworthy that the magnetic exchange parameters are very similar despite the significantly different spin values and spin dimension.

Previous studies (22) have identified the ordering in $Mn(O_3PC_6H_5)\cdot H_2O$ as a transition to a canted antiferromagnetic state in analogy to other manganese organophosphonates (15). The magnetic moments assume a noncollinear orientation that produces a weak ferromagnetic moment that lies within the plane of the manganese ions. This moment, and hence the transition from the paramagnetic to the canted antiferromagnetic state, can be observed in a difference plot of the magnetization as a function of temperature for experiments performed in field-cooled (fc) and zero-field-cooled (zfc) conditions, ΔM_{fc-zfc} (Fig. 5). The ordering temperature, T_N, may be identified in the M_{fc} data as the temperature where the magnetization begins to deviate from its high-temperature paramagnetic behavior, and from Fig. 5, $T_N = 11.7$ K for $Mn(O_3PC_6H_5)\cdot H_2O$. Another parameter, T_N^*, is defined as the temperature at which ΔM_{fc-zfc} differs significantly from 0. These two temperatures, $T_N = 11.7$ K and $T_N^* = 11.5$ K, are identifiable in Fig. 5. The value of T_N^* changes as a function of the magnitude of the applied measuring field and as a result, for small values of T_N, it is best to acquire data with a smaller measuring field, typically 50–100 G. Due to this dependence upon the measuring field, it is important to realize that T_N^* will always be lower than T_N, but T_N^* is nevertheless evidence of an ordered state with a weak ferromagnetic moment. In contrast to the weakly ferromagnetic manganese compound, the pure cobalt compound is antiferromagnetic with $T_N = 3.9$ K, as determined from both dc magnetization and ac susceptibility measurements.

Magnetic properties of the solid solutions. Typical magnetization plots for the solid solutions $Mn_xCo_{1-x}(O_3PC_6H_5)\cdot H_2O$ with $0.25 < x < 1.00$ are shown in Fig. 6. The ordering temperatures identified in the magnetization vs temperature plots are consistent, within experimental

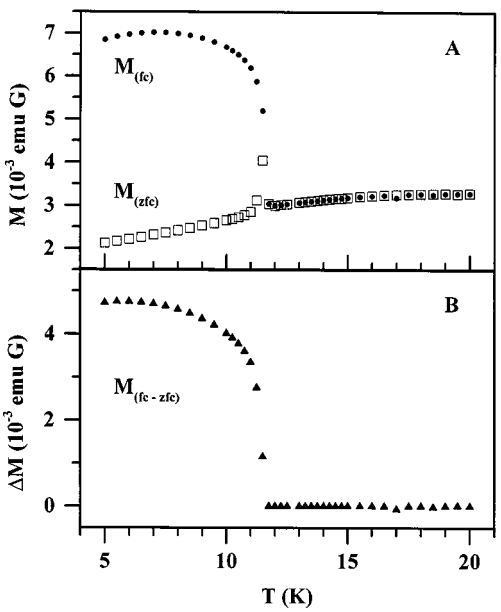

FIG. 5. (A) Field-cooled (FC) and zero-field-cooled (ZFC) magnetization data of manganese phenylphosphonate are shown as a function of temperature. Both data sets were acquired with a 100-G measuring field. (B) The difference between field-cooled and zero-field-cooled magnetization versus temperature for $Mn(O_3PC_6H_5)\cdot H_2O$ measured in a field of 100 G.

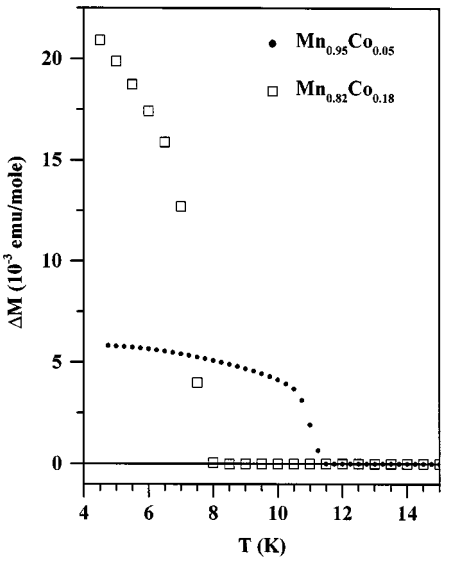

FIG. 6. The difference between the field-cooled and zero-field-cooled magnetization, ΔM, is shown as a function of temperature. Typical data from the Mn-rich (i.e., $x > 0.25$) samples are shown when the magnetic field, for measuring and field cooling, was 100 G.

resolution, with the temperatures of anomalies in the ac susceptibility studies. Like the pure $Mn(O_3PC_6H_5)\cdot H_2O$, the solid solutions with $x > 0.25$ form canted antiferromagnets in the low-temperature state. For $x < 0.25$, the ΔM_{fc-zfc} vs temperature plots still reveal the ordering temperature, but the magnitude of ΔM_{fc-zfc} is much smaller and negative, Fig. 7. This point is discussed further, later in this section. Nonetheless, the ordering temperatures were confirmed with ac susceptibility measurements, and they are included in Fig. 8.

The mixed Mn/Co phenylphosphonates can be thought of as magnetically doped pure manganese or pure cobalt lattices with the other metal ion as impurity. Consequently, a reduction of T_N from the pure systems is anticipated. Since the magnetic exchange interactions and lattices are similar, the primary differences are the spin values and the dimension of the spins (i.e., Ising-like or Heisenberg-like). Therefore, the reduction of T_N is not expected to be as strong as it is for the case of doping with diamagnetic spins, and these general tendencies are reflected in the phase diagram in Fig. 8. In the Mn-rich regime, $T_N(x)$ closely follows a linear function with an $x = 0$ intercept (solid line) at the T_N value obtained for the pure Co material. For $0.25 < x < 0.60$, the perturbation of the magnetic correlations is stronger as the percolation threshold is approached and the reduction of T_N follows a trend qualitatively represented by the dotted line. For the Co-rich samples, there is not sufficient resolution in the identification of T_N to allow a specific x dependence to be identified, so the general trend is sketched by the dashed line. The prediction of a tetracritical point at $x = 0.25$ agrees well with a face-centered square planar lattice containing four nearest neighbors where one spin species dominates the magnetic exchange. In our case, the Mn^{2+} spins dominate the local magnetic environment. Tetracritical points (34, 50) have been observed previously in other doped magnetic systems containing competing magnetic anisotropies (51–54).

SEARCH FOR SPIN GLASS OR PRECURSOR PHASES

The assignment of the pure Mn^{2+} material as a canted antiferromagnetic $S = \frac{5}{2}$ Heisenberg-like system and the pure Co^{2+} system as a quantum antiferromagnetic $S = \frac{1}{2}$ Ising-like system opens the possibility of forming a spin-frustrated state in a randomly mixed Mn/Co system. In molecular magnetism, similar studies on layered materials have been reported. Thus, bimetallic oxalato layered mixed-metal compounds containing competing ferro- and antiferromagnetic interactions have been magnetically characterized and in some cases spin glass behavior has been observed (55). Spin-frustrated systems displaying magnetic properties characteristic of spin glasses have also been

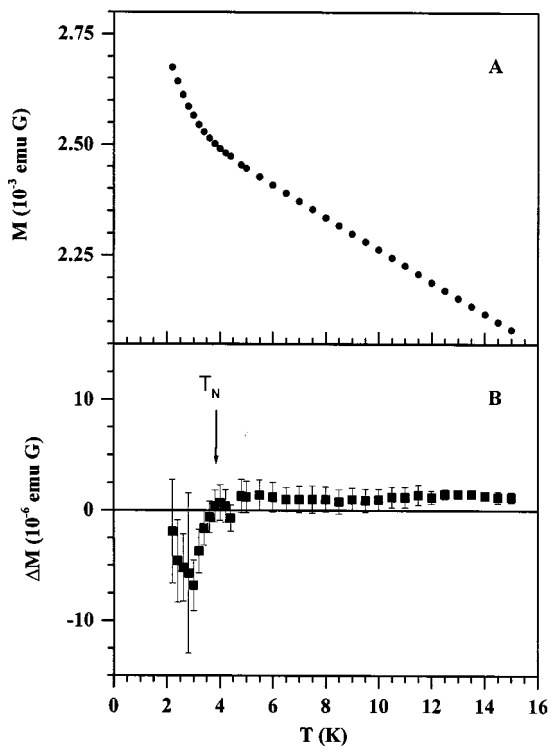

FIG. 7. (A) Field-cooled and zero-field-cooled dc magnetization for $x = 0.1$. Both data sets were acquired with a 100-G measuring field, and on this scale, the difference between the two data sets is not visually detectable. (B) The difference between field-cooled and zero-field-cooled magnetization from (A) is shown as a function of temperature. The onset of a negative magnetization occurs at T_N, and this signature is characteristic for all the Co-rich (i.e., $x < 0.25$) samples.

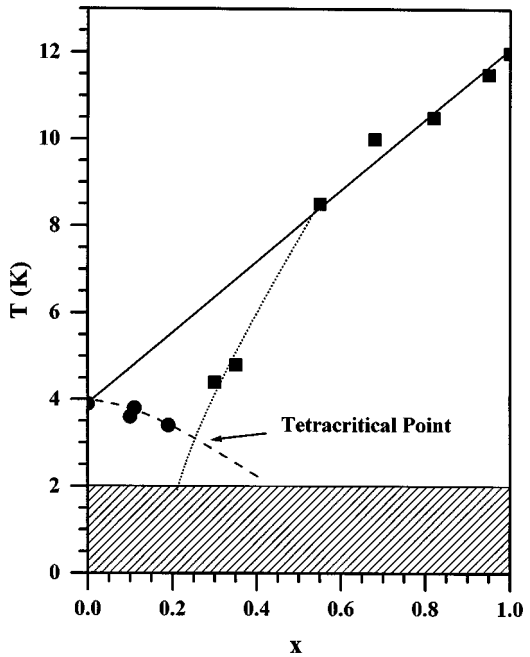

FIG. 8. The magnetic phase diagram of $Mn_xCo_{1-x}(O_3PC_6H_5)\cdot H_2O$ indicating the ordering temperature vs Mn^{2+} concentration. The phase diagram has a tetracritical point at $x = 0.25$, as described in the text. The present work was restricted to $T > 2$ K. The lines are guides for the eyes and are described in the text.

observed in doped magnetic materials possessing tetracritical points in their magnetic phase diagrams (35, 38, 56).

Time-dependent thermal remnant magnetization studies were performed with two samples, $x = 0.30$ and 0.68. In one set of experiments, the samples were zero-field cooled from 300 K to 5, 7, and 12 K in three separate runs. The process of cooling from 300 K to the low-temperature fixed point required approximately 80 min. After equilibrium was established, a field of 1 kG was applied, and the magnetization was monitored for nominally 40 min. During this time, the magnetization was observed to relax toward an equilibrium value, and this process was easily fitted by a simple exponential function, yielding time constants ranging from 700 to 1100 s. In a different measurement, the magnetization relaxation rates of the sample holders were studied and were determined to be negligible. The total change of the signal during the measurement after achieving the equilibrium state, as defined by the thermometer of the instrument, was about 1%. Although these results may be suggestive of behavior associated with a spin glass state, we consider them to be related to the process of cooling the powder samples. A simple cooling model (57) provides a plausible explanation for the measured relaxation rates. It is noteworthy that the same type of behavior was observed for both samples and at all three of the temperatures that were studied. In other words, the experiments covered several of the magnetic phases shown in Fig. 8, and in every instance, the behavior was always the same.

In a second set of studies, the ac susceptibility of samples was investigated. The temperature dependences of the real component of the ac susceptibility in applied magnetic fields of 0 and 1 kG are shown in Fig. 9 for $x = 0.82$. Our ac studies of all x reproduced, to within experimental resolution, the ordering temperatures seen in the dc magnetization data. However, when no external DC magnetic field was present, new peaks were observed in the ac susceptibility signals, and these features were not present in the dc magnetization data. Upon application of a 1 kG field, these features were suppressed and, therefore, can be attributed to the dynamics of the magnetic domains and the powder nature of the specimens. The temperatures of the transitions as measured by ac susceptibility did not appear to be frequency dependent from 17 Hz to 1.5 kHz. Therefore, no spin glass behavior was observed in any of the samples at any temperature $T > 2$ K.

In summary, no evidence of a spin glass state was obtained in our measurements. It is important to note, however, that a spin-flop transition has been observed in pure $Mn(O_3PC_6H_5)\cdot H_2O$ in magnetization vs field studies performed at 2 K (22), and a similar spin-flop transition is seen for the solid solution with $x = 0.84$. However, no spin-flop signatures were observed for samples with $x < 0.84$, where an increasing intrinsic background arising from competing magnetic spins may have masked the spin-flop transitions. Furthermore, we were particularly curious about the possibility of precursor behavior in the region near the tetracritical point, i.e., a region bounded by the solid, dotted, and

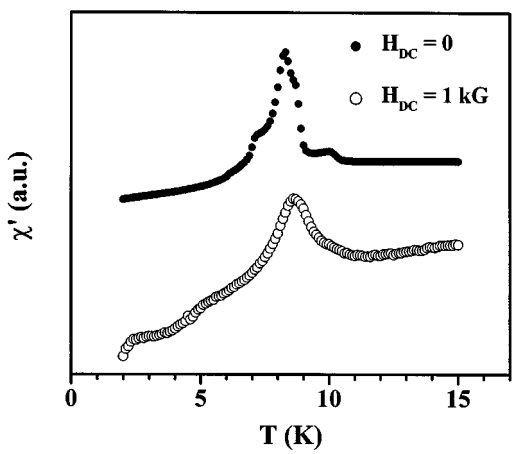

FIG. 9. The real component of the ac susceptibility for $Mn_{0.18}Co_{0.82}(O_3PC_6H_5)\cdot H_2O$ at 17 Hz and an amplitude of 4 G. The ac susceptibility was studied in an applied field of 0 and 1 kG, corresponding to the filled and open circles, respectively. The identification of T_N is consistent with the values determined by dc magnetization techniques. The ac response is understood as arising from the dynamics of the magnetic domains and the powder nature of the specimens, as described in the text.

broken lines in Fig. 8. However, as discussed at the beginning of this section, no magnetic glassy behavior was observed in this region. Finally, we note that for $x = 0.30$ and 0.35, our studies down to 2 K did not reveal any anomalies indicative of crossing into an "intermediate" phase (34). Naturally, specific heat studies may provide additional information concerning the existence of and the identification of such a phase.

Negative magnetization in the cobalt-rich samples. For $x < 0.25$, ordering is observed, but the value of $\Delta M_{\mathrm{fc-zfc}}$ is small and negative, Fig. 7. Features in the ac susceptibility are observed at the same temperatures, so we associate these temperatures with the transition to long-range antiferromagnetic order. The negative magnetization shifts observed for the Co-rich specimens contrast with the positive magnetization shifts detected for the Mn-rich materials. The phenomenon of negative magnetization has been identified previously in a variety of ferrimagnetic materials (41, 42). Naturally with the doped Co-rich specimens, similar arguments may be made if small regions of ferrimagnetic ordered phase are present. However, negative magnetization is also observed in the pure Co material, although it is even weaker than observed in the data shown in Fig. 7B. Negative magnetization has previously been observed in the canted antiferromagnet $LaVO_3$ (58), and the same phenomenon may be responsible for the behavior observed for the cobalt phase ($x < 0.25$).

CONCLUSION

A new series of mixed metal phenylphosphonate solid solutions, $Mn_xCo_{1-x}(O_3C_6H_5)\cdot H_2O$, have been prepared and their magnetic properties investigated. Each composition undergoes long-range magnetic ordering to a canted antiferromagnetic state at temperatures, $T_N \leq 12$ K, and a magnetic phase diagram has been constructed based on individual dc and ac susceptibility measurements. For both the Mn^{2+} and Co^{2+} high concentration limits, T_N decreases relative to the pure single-ion phosphonates, consistent with what is expected for magnetic ion impurity doping. The phase diagram includes four phases with a tetracritical point at $x = 0.25$ K, indicating a competition between the Heisenberg-like Mn^{2+} and the Ising-like Co^{2+} spins, with the $S = \frac{5}{2}$ Mn^{2+} dominating the local environment. While prior studies on mixed-metal systems possessing competing spin types have shown evidence for spin glass behavior, no such state is observed in the $Mn_xCo_{1-x}(O_3C_6H_5)\cdot H_2O$ solid solutions.

ACKNOWLEDGMENTS

During the course of this work, we have benefited from conversations with A. Feher, M. Orendáč, and A. Orendáčova. This research was supported by the National Science Foundation through Grants DMR-9900855 (D.R.T.), INT-9722935 (M.W.M), and DMR-9704225 (M.W.M). Special thanks are given to the Florida Major Analytical Instrumentation Center for use of XRD facilities and to Dr. Katherine Williams and Mr. Russell Pierce for use of the atomic absorption spectrometer.

REFERENCES

1. A. Clearfield and G. D. Smith, *Inorg. Chem.* **8,** 431–436 (1969).
2. A. Clearfield, *Chem. Rev.* **88,** 125–148 (1988).
3. G. Alberti, U. Costantino, S. Allulli, and N. Tomassini, *J. Inorg. Nucl. Chem.* **40,** 1113–1117 (1978).
4. G. Cao, H. Lee, V. M. Lynch, and T. E. Mallouk, *Solid State Ionics* **26,** 63–69 (1988).
5. G. Cao, H. Lee, V. M. Lynch, and T. E. Mallouk, *Inorg. Chem.* **27,** 2781–2785 (1988).
6. D. Cunningham and P. J. D. Hennelly, *Inorg. Chim. Acta* **37,** 95–102 (1979).
7. Y. Ortiz-Avila, P. R. Rudolf, and A. Clearfield, *Inorg. Chem.* **28,** 2137–2141 (1989).
8. G. Cao, H.-G. Hong, and T. E. Mallouk, *Acc. Chem. Res.* **25,** 420–427 (1992).
9. H. E. Katz, M. L. Schilling, C. E. D. Chidsey, T. M. Putvinski, and R. S. Hutton, *Chem. Mater.* **3,** 699–703 (1991).
10. H. E. Katz, G. Scheller, T. M. Putvinski, M. L. Schilling, W. L. Wilson, and C. E. D. Chidsey, *Science* **254,** 1485–1487 (1991).
11. H. E. Katz, W. L. Wilson, and G. Scheller, *J. Am. Chem. Soc.* **116,** 6636–6640 (1994).
12. M. B. Dines and P. M. DiGiacomo, *Inorg. Chem.* **20,** 92–97 (1981).
13. D. M. Poojary, L. A. Vermeulen, E. Vicenzi, A. Clearfield, and M. E. Thompson, *Chem. Mater.* **6,** 1845–1849 (1994).
14. D. Visser, S. G. Carling, P. Day, and J. Deportes, *J. Appl. Phys.* **69,** 6016–6018 (1991).
15. S. G. Carling, P. Day, D. Visser, and R. K. Kremer, *J. Solid State Chem.* **106,** 111–119 (1993), doi:10.1006/jssc.1993.1269.
16. S. G. Carling, P. Day, and D. Visser, *J. Phys.: Condens. Matter.* **7,** L109–L113 (1995).
17. S. G. Carling, P. Day, and D. Visser, *Inorg. Chem.* **34,** 3917–3927 (1995).
18. P. Rabu, P. Janvier, and B. Bujoli, *J. Mater. Chem.* **9,** 1323–1326 (1999).
19. J. Le Bideau, C. Payen, B. Bujoli, P. Palvadeau, and J. Rouxel, *J. Magn. Magn. Mater.* **140–144**, 1719–1720 (1995).
20. B. Bujoli, O. Pena, P. Palvadeau, J. Le Bideau, C. Payen, and J. Rouxel, *Chem. Mater.* **5,** 583–587 (1993).
21. P. Gerbier, C. Guerin, J. Lebideau, and K. Valle, *Chem. Mater.* **12,** 264–267 (2000).
22. G. E. Fanucci, J. Krzystek, M. W. Meisel, L.-C. Brunel, and D. R. Talham, *J. Am. Chem. Soc.* **120,** 5469–5479 (1998).
23. G. E. Fanucci, M. A. Petruska, M. W. Meisel, and D. R. Talham, *J. Solid State Chem.* **145,** 443–451 (1999), doi:10.1006/jssc.1999.8145.
24. H. Byrd, J. K. Pike, and D. R. Talham, *Chem. Mater.* **5,** 709–715 (1993).
25. H. Byrd, S. Whipps, J. K. Pike, J. Ma, S. E. Nagler, and D. R. Talham, *J. Am. Chem. Soc.* **116,** 295–301 (1994).
26. H. Byrd, J. K. Pike, and D. R. Talham, *Syn. Met.* **71,** 1977–1980 (1995).
27. G. E. Fanucci, C. M. Nixon, M. A. Petruska, C. T. Seip, D. R. Talham, G. E. Granroth, and M. W. Meisel, *in* "Supramolecular Engineering of Synthetic Metallic Materials" (J. Veciana and C. Rovira, Eds.), Vol. 518, pp. 465–475, 1998.
28. G. E. Fanucci, C. T. Seip, M. A. Petruska, S. Ravaine, C. M. Nixon, and D. R. Talham, *Thin Solid Films* **327–329,** 331–335 (1998).
29. G. E. Fanucci and D. R. Talham, *Langmuir* **15,** 3289–3295 (1999).

30. M. A. Petruska, G. E. Fanucci, and D. R. Talham, *Chem. Mater*. **10,** 177–189 (1998).
31. M. A. Petruska, G. E. Fanucci, and D. R. Talham, *Thin Solid Films* **327–329,** 131–135 (1998).
32. M. A. Petruska and D. R. Talham, *Chem. Mater*. **10,** 3673–3682 (1998).
33. M. A. Petruska and D. R. Talham, *Langmuir* **16,** 5123–5129 (2000).
34. L. J. de Jongh, *in* "Magnetic Properties of Layered Transition Metal Compounds" (L. J. de Jongh, Ed.), pp. 1–51. Kluwer Academic, Dordrecht, 1990.
35. G. V. Rubenacker, D. P. Raffaell, J. E. Drumheller, and K. Emerson, *Phys. Rev. B* **37,** 3563–3568 (1988).
36. K. Zenmyo and H. Kubo, *J. Phys. Soc. Jpn.* **64,** 1320–1325 (1995).
37. G. C. DeFotis, G. S. Coker, J. W. Jones, C. S. Branch, H. A. King, J. S. Bergman, S. Lee, and J. R. Goodey, *Phys. Rev. B* **58,** 12,178–12,192 (1998).
38. G. C. DeFotis, E. M. Just, V. J. Pugh, G. A. Coffey, B. D. Hogg, S. L. Fitzhenry, J. L. Marmorino, D. J. Krovich, and R. V. Chamberlain, *J. Magn. Magn. Mater*. **202,** 27–46 (1999).
39. G. C. DeFotis, D. S. Mantus, E. M. McGhee, K. R. Echols and R. S. Weis, *Phys. Rev. B* **38,** 11,486–11,499 (1988).
40. J. A. Mydosh, "Spin Glasses: An Experimental Introduction." Taylor & Franacis, London, 1993.
41. C. J. Nuttall and P. Day, *Chem. Mater*. **10,** 3050–3057 (1998).
42. H. C. Nguyen and J. B. Goodenough, *Phys. Rev. B* **52,** 8776–8787 (1995).
43. G. E. Fanucci, J. T. Culp, B. C. Watson, R. Backov, H. Ohnuki, D. R. Talham, and M. W. Meisel, *Physica B* **284–288,** 1499–1500 (2000).
44. P. J. C. Signore, Ph.D. thesis, University of Florida, 1994.
45. B. H. Ward, G. E. Granroth, K. A. Abboud, M. W. Meisel, P. G. Rasmussen, and D. R. Talham, *J. Mat. Chem*. **8,** 1373–1378 (1998).
46. C. T. Seip, H. Byrd, and D. R. Talham, *Inorg. Chem.* **35,** 3479–3483 (1996).
47. M. E. Lines, *J. Phys. Chem. Solids* **31,** 101–116 (1970).
48. M. F. Sykes and M. Fischer, *Physica* **28,** 919–938 (1962).
49. R. Navarro, *in* "Magnetic Properties of Layered Transition Metal Compounds" (L. J. de Jongh, Ed.), pp. 105–190. Kluwer Academic, Dordrecht, 1990.
50. S. Fishman and A. Aharony, *Phys. Rev. B* **18,** 3507–3520 (1978).
51. K. Katsumata, M. Kobayashi, T. Sato, and Y. Miyako, *Phys. Rev. B* **19,** 2700–2703 (1979).
52. L. Brevaart, E. Frikkee, and L. J. de Jongh, *Solid State Comm.* **25,** 1031–1033 (1978).
53. K. Katsumata, S. M. Shapiro, G. Shirane, and J. Tuchendler, *Phys. Rev. B* **46,** 14,906–14,908 (1992).
54. P. Wong, P. M. Horn, R. J. Birgeneau, and G. Shirane, *Phys. Rev. B* **27,** 428–447 (1983).
55. E. Coronado, J. R. Galán-Mascarós, C. J. Gómez-García, and J. M. Martínez-Agudo, *Adv. Mater*. **11,** 558–561 (1999).
56. G. C. DeFotis, P. Christoph, and P. A. Spencer, *J. Chem. Phys* **80,** 2079–2086 (1984).
57. R. C. Richardson and E. N. Smith, "Experimental Techniques in Condensed Matter Physics at Low Temperatures," Sec 3.5. Addison-Wesley, Redwood City, CA, 1988.
58. H. C. Nguyen and J. B. Goodenough, *Phys. Rev. B* **52,** 324–334 (1995).